Journal of Nuclear Medicine, published on June 12, 2020 as doi:10.2967/jnumed.119.233163

PET imaging of the natural killer cell activation receptor NKp30

Travis M. Shaffer[1], Amin Aalipour[2], Christian M. Schürch[3], Sanjiv S. Gambhir[1,2,4,*]

1. Department of Radiology, Stanford University, Stanford CA, 94305
2. Department of Bioengineering, Stanford University, Stanford CA, 94305
3. Department of Microbiology & Immunology, Stanford University, Stanford, CA, 94305
4. Bio-X Program and Molecular Imaging Program at Stanford (MIPS), Stanford University, Stanford CA, 94305

Corresponding author:

Sanjiv S. Gambhir, M.D., Ph.D.

Clark Center, 318 Campus Drive, Rm-E150, Stanford CA 94305

sgambhir@stanford.edu

Tel: +1 650-725-2309

First author:

Travis M. Shaffer, Ph.D.

Clark Center, 318 Campus Drive, Rm-E150, Stanford CA 94305

tshaffer@stanford.edu

Tel: +1 650-724-3624

Running title: PET imaging of NKp30

Word count: 5768

Abstract

Redirecting the immune system in cancer treatment has led to remarkable responses in a subset of patients. Natural killer (NK) cells are innate lymphoid cells being explored as they engage tumor cells in different mechanisms compared to T cells, which could be exploited for treatment of non-responders to current immunotherapies. NK cell therapies are monitored through measuring peripheral NK cell concentrations or changes in tumor volume over time. The former does not detect NK cells at the tumor site(s), and the latter is inaccurate for immunotherapies because of pseudoprogression. Therefore, new imaging methods are required as companion diagnostics for optimizing immunotherapies. **Methods:** Here we develop and complete pre-clinical *in vivo* validation of two antibody-based PET probes specific for NKp30, an activation natural cytotoxicity receptor expressed by human NK cells. Quantitative, multicolor flow cytometry during a variety of NK cell activation conditions was completed on primary human NK cells and the NK92MI cell line. Human renal cell carcinoma (RCC) tumors were stained for the NK cell receptors CD56, NKp30, and NKp46 to determine expression on tumor-infiltrating NK cells. An NKp30 antibody was radiolabeled with ^{64}Cu or ^{89}Zr and evaluated in subcutaneous xenografts and adoptive cell transfer mouse models. **Results:** Quantitative flow cytometry showed consistent expression of the NKp30 receptor during different activation conditions. NKp30 and NKp46 co-stained in RCC samples, demonstrating the expression of these receptors on tumor-infiltrating NK cells in human tumors, while tumor cells in one RCC sample expressed the peripheral NK marker CD56. Both PET tracers showed high stability and specificity *in vitro* and *in vivo*. Notably, ^{89}Zr-NKp30Ab had higher on-target contrast compared to ^{64}Cu-NKpAb at their respective terminal time points. ^{64}Cu-NKp30Ab

delineated NK cell trafficking to the liver and spleen in an adoptive cell transfer model. **Conclusion:** The consistent expression of NKp30 on NK cells makes it an attractive target for quantitative imaging. Immunofluorescence staining on human RCC samples demonstrated the advantages of NKp30 targeting versus the traditional CD56 for detection of tumor infiltrating NK cells. This work advances PET imaging of NK cells and supports the translation of imaging agents for immunotherapy monitoring.

Keywords: Natural Killer, NK, NKp30, immune cell imaging, innate lymphoid cell, cancer immunotherapy

INTRODUCTION

Redirecting the immune system to detect and destroy malignancies has resulted in remarkable responses in a subset of cancers(*1,2*). However, the moderate success rates of these therapies, associated costs (often > $100,000/year)(*3*), and potential adverse side effects such as cytokine release syndrome(*4*) have led to exploration into new strategies to aid the immune system against cancer. One such strategy modulates natural killer (NK) cells, important innate lymphoid cells that are the first immunological defenders against viral and cancer threats(*5*). NK cells kill target cells without the need for prior sensitization and interact with their environment via a complex integration of signals from an array of receptors. As NK cells can detect the absence of major histocompatibility complex 1, they can destroy cancer cells that escape detection by T cells through the downregulation of this receptor(*6-9*). They are also the main cell type responsible for antibody-dependent cellular cytotoxicity(*10,11*).

Therapeutic strategies utilizing NK cells include both adoptive cell transfer and modulating NK response *in situ*(*12*). Therapeutic response is gauged using computed tomography (CT)/magnetic resonance imaging (MRI) or analysis of circulating NK cells via flow cytometry(*13*). Measuring changes in tumor volume via CT/MR has limited prognostic value for immunotherapies due to the influx of effector cells in the tumor microenvironment leading to pseudoprogression. Likewise, circulating NK cell concentration is a poor surrogate for NK cell engagement and activation at desired sites of therapeutic action. New approaches are needed to non-invasively monitor NK cell localization and activation to better predict therapy responses, shed light of mechanisms

of therapeutic failure, and facilitate the clinical translation of emerging NK cell cancer therapies.

For both allogeneic and autologous adoptive cell transfer (ACT) therapies a variety of methods are available for quantitative imaging through *ex vivo* labeling with ^{111}In-oxine(*14*), ^{89}Zr-oxine(*15,16*), or PET reporter gene methods(*17*). However, there is currently a lack of endogenous NK cell imaging agents to use as companion diagnostics for therapies that modulate endogenous NK cells and can also be used with adoptive cell therapies(*5*). An ideal endogenous NK imaging biomarker is a receptor that is both highly and specifically expressed on activated cells. One study imaged the human CD56 receptor with a ^{99m}Tc-radiolabeled antibody for single photon emission computed tomography (SPECT) (*18*). However, CD56 is expressed on numerous cell types including T cells, NK cells, dendritic cells, and monocytes, along with a subset of cancers including glioma, renal cell carcinoma (RCC), and pancreatic cancer(*19,20*), thus potentially precluding its use for specifically imaging tumor-infiltrating NK cells. Additionally, CD56 has a dim expression in NK cells with high cytotoxic activity, and high expression in NK cells that have an immunoregulatory role(*21*).

The natural cytotoxicity receptors (NCRs) are all activation receptors specifically expressed on human NK cells (along with rare innate lymphoid subsets)(*22,23*). Among NCRs, activating ligands for NKp30 are the most widely known, such as the tumor ligand B7-H6. Intense NKp30 immunohistochemistry staining has been shown to be a positive response indicator of survival in a variety of cancers, including acute myeloid leukemia(*24*), gastric cancer(*25*), and cervical cancer(*26*). To establish the utility of NKp30 as an imaging biomarker, we performed quantitative flow cytometry on human NK

cells to determine the number of NCRs available for imaging, stained for NKp30 expression in human tumor samples, and developed two antibody-based positron emission tomography (PET) tracers specific for NKp30 for *in vivo* imaging in both tumor xenografts and ACT models.

MATERIALS AND METHODS

Human NK cell isolation and culturing

Human buffy coats were obtained from the Stanford blood bank. Peripheral blood mononuclear cells (PBMCs) were isolated using a Sepmate-50 kit (StemCell Tech). Human NK cells were isolated from PBMCs using a negative selection magnetic bead kit specific for human NK cells (StemCell Tech). Cells were grown in 12-well plates using NK MACS medium (Miltenyi) supplemented with human serum and IL-2 for 4 days prior to use. NK92MI and primary human NK cells were activated with the addition of NK activation beads (Miltenyi) at a 2:1 bead to cell ratio or with phorbol 12-myristate 13-acetate (50ng/mL) and Ionomycin (0.5 µg/ml). Flow cytometry was completed 24 h post-activation.

Flow cytometry on NK cells

Quantitative flow cytometry on transfected HeLa cells was completed using a Qifikit (Agilent) per kit instructions with one alteration. An APC F(ab')2-Goat anti-Mouse IgG (H+L) Secondary Antibody (Thermo Fisher) was used rather than the kit-provided Fluorescein isothiocyanate (FITC) secondary antibody due to the HeLa-NKp30 cell line expressing GFP. NK92MI and primary NK cell receptor quantification was conducted using kits from BangsLabs. Quantifying NKp30 receptors on the HeLa-NKp30 cell line was completed Quantification of the NK92MI and primary human NK cells using MESF

calibration beads for PE and APC fluorophores. Cells were stained with DAPI, FITC-CD3, PE-NKp30Ab, APC-NKp46Ab, and PerCp-Vio700 CD56 per manufacturer recommendations. Fc block (BD biosciences) was used to prevent non-specific antibody binding, thus precluding the use of the QiFikit (which uses secondary staining) for quantification flow. Flow cytometry was completed using an LSR II instrument (BD Biosciences). Compensation beads, isotype controls, and FMOs were used for data analysis and gating. Data were analyzed using FlowJo (TreeStar).

Immunofluorescence staining

Fresh-frozen renal cell carcinoma patients' samples embedded in optimal cutting temperature medium (VWR / Sakura cat. no. 25680-930) were sectioned to 7□m thickness on a cryostat (Leica), mounted onto glass coverslips (22x22 mm, # 1 ½, Electron Microscopy Sciences cat. no. 72204-01) pre-coated with poly-L-lysine (Sigma-Aldrich cat. no. P8920-500ML), air dried, and stored at -80 °C.

Staining buffers were prepared and procedures were performed as previously described(*27*), with slight modifications. Briefly, tissues were recovered from -80 °C on drierite desiccant (Thermo Fisher cat. no. 07-578-3A) for 2 min at room temperature, followed by incubation in acetone for 10 min. Tissues were then dried for 2 min in a humidity chamber, hydrated in staining solution 1 (S1), and fixed in S1 containing 1.6% paraformaldehyde (PFA, Thermo Fisher, cat. no. 50-980-487) for 10 min. After fixation, sections were washed in S1, followed by equilibration in staining solution 2 (S2). Non-specific binding was blocked by incubating the sections in blocking buffer (50ug/ml mouse IgG [Sigma-Aldrich cat. no. I5381] and 50 ug/ml rat IgG [Sigma-Aldrich cat. no. I4131] in S2) for 10min at RT. The staining cocktail was prepared in blocking buffer using the

following antibodies: mouse anti-human NKp46-AlexaFluor488 (Biolegend cat. no. 331937, dilution 1:50), mouse anti-human CD56-PE (Biolegend cat. no. 362524, dilution 1:100) and mouse anti-human NKp30-APC (R&D Systems cat. no. FAB1849A-025, dilution 1:20). Sections were stained for 2 h at RT, washed in S2 for 5 min, and fixed with 1.6% PFA in staining solution 4 (S4) for 10 min at RT. Nuclei were counterstained with Hoechst 33342 (Thermo Fisher cat. no. 62249, dilution 1:1000), and coverslips were mounted onto glass slides using Cytoseal XYL mounting medium (Thermo Fisher 8312-4). Hematoxylin & eosin stained sections were prepared using standard pathology procedures. Images were acquired on a Keyence BZ-X710 inverted fluorescence microscope equipped with a 40x Plan Fluor oil objective and processed using ImageJ/FIJI.

NK cell kill assay

MeWo or SK-Mel-28 human melanoma cells expressing firefly luciferase were seeded in 96 well plates at 10,000 cells per well. 24 h after seeding, 10,000 NK92MI cells with or without the NKp30Ab were added to the wells, along with NKp30Ab alone and control wells with only tumors cells. NKp30Ab diluted in PBS was added at 10,000 or 100,000 antibodies per NK cell. Luciferase imaging was performed at 24 h post cell incubation to assess the killing capabilities of the NK92MI cell line using an IVIS system (Perkin Elmer) upon addition of D-Luciferin (0.3 mg/ml final concentration).

Cell culture and transfection of NKp30 receptor

The human NK cell line NK92MI and HeLa human cervical carcinoma cells were obtained from American Type Culture Collection (ATCC). NK92MI (human NK) cells were cultured in RPMI supplemented with 20 % FBS, 1 % antibiotic-antimycotic, and 0.1 mM

2-mercaptoethanol. HeLa cells were cultured in Dulbecco modified Eagle medium supplemented with 10% fetal bovine serum and 1% antibiotic-antimycotic. A plasmid was obtained from VectorBuilder consisting of the human NKp30 (NCR1) sequence driven by the EF1α promoter, eGFP and the puromycin resistant gene were driven by the CMV for selection of stable cells (Supplemental Fig. 1A). HeLa cells were transfected using a Lipofectamine 3000 kit (ThermoFisher). Transfected HeLa cells (HeLa-NKp30) were placed under selection with the addition of 40 μg/mL puromycin and sorted three times with the top 2% of PE-NKp30Ab$^+$GFP$^+$ cells collected to generate a stable line (Supplemental Fig. 1B). All cell culture reagents were obtained from ThermoFisher Scientific.

DOTA and DFO conjugation to NKp30 antibody

A low endotoxin, azide-free purified (clone P30-15) monoclonal mouse IgG1 antibody specific for the human NKp30 receptor (NKp30Ab) along with the corresponding mouse isotype control (IgG1, κ isotype control clone MOPC-12) was purchased from Biolegend. The antibodies were buffer exchanged into PBS pH=8.5 and DOTA-NHS ester added (1 mg/mL) at a molar ratio of 20:1 and incubated overnight at 4°C. The DOTA-NKp30Ab was purified using 50kDa spin filtration with three washes in 0.1M ammonium acetate, pH=5. For DFO conjugation, NKp30Ab (1 mg/mL) was buffer exchanged into PBS pH=8.5 followed by the addition of DFO-SCN at a 20:1 or 40:1 ratio. This was allowed to conjugate for 2 h at 37 °C followed by 50kD spin filtration and washing three times in PBS pH=7.3.

Radiolabeling NKp30Ab

$^{64}CuCl_2$ in 0.1N HCl was obtained from the University of Wisconsin with a specific activity of 17.76-162.8 GBq/μmol. This was added to DOTA-NKp30Ab at a ratio of 0.37 MBq/μg and a final pH of 5 and incubated at 37°C for 30 min. This was followed by the addition of 5μL of 50mM EDTA for 10 min to scavenge free ^{64}Cu. Purification was achieved by spin filtration and three washes at 25°C, with final resuspension in saline. Instant thin-layer chromatography (iTLC) with 50 mM citric acid as the mobile phase and size exclusion HPLC were completed to validate purity and specific activity, respectively. ^{89}Zr-oxalate was obtained from the University of Alabama at a specific activity of 59.2-103.6 GBq/μmol. This was neutralized with 1.0 M sodium carbonate and added to DFO-NKp30Ab at a ratio of 0.185 MBq/μg. This was incubated at 37 °C for 60 min followed the addition of 5 μL of 50 mM EDTA for removal of free ^{89}Zr. Purification was achieved as described for DOTA-NKp30Ab. iTLC was completed on the crude and purified product with 50 mM EDTA as the mobile phase.

***In vitro* immunoreactivity and serum stability assays**

3.7 MBq of ^{64}Cu-NKp30Ab or ^{89}Zr-NKp30Ab along with isotype controls in 10 μl of saline was incubated in 100 μl of mouse or human serum at 37 °C. 1μL samples (N=5) were taken every 24 h for iTLC. Immunoreactivity assays for ^{64}Cu-NKp30Ab and ^{89}Zr-NKp30Ab were completed as previously described(*28*). 0.037 MBq of the tracer was added to a serial dilution of NKp30-expressing HeLa cells, incubated for 30 min, and washed twice in PBS prior to gamma counting. To assess specificity in human NK cells, 5 $x10^5$ NK92MI or human NK cells were incubated with each tracer or isotype control and processed as above.

***In Vivo* Xenograft Imaging and Biodistribution studies**

Nu/nu female mice were supplied by Charles River. When mice were 6-10 weeks of age, 5 x10^5 NKp30-expressing HeLa cells were mixed with 100 μL Matrigel and injected in the left flank subcutaneously, while in the right flank equivalent number of NKp30-negative HeLa cells mixed with Matrigel were injected. Xenografts were allowed to grow for 10-14 days prior to PET studies. 2.96-4.44 MBq (10-15μg) of ^{64}Cu-NKp30Ab or 1.85-3.7 MBq (10-20 μg) of ^{89}Zr-NKp30Ab were injected intravenously in 100μL of saline via tail vein at 14:00-18:00. PET imaging was conducted every 24 h out to 48 h for ^{64}Cu-NKp30Ab or 120 h for ^{89}Zr-NKp30Ab. Mice were anesthetized using 2.5% isoflurane delivered in 100% oxygen for imaging. PET/CT scans were completed on an Inveon PET/CT with scan times of 10 min for 24 h time and 20-30 min for subsequent time points. PET/CT image reconstruction was completed using Inveon software with attenuation corrections applied. Experiments were completed on two separate occasions (n=3-4 per run). All experiments were approved by the Stanford Administrative Panel on Laboratory Animal Care (APLAC) committee (#32843). A paired t-test was used to compare the statistical differences in tracer update in NKp30 positive and negative tumor xenografts. A power calculation was completed with 90% power, α=0.05, and assuming normal distribution to determine the number of mice per cohort.

***In Vivo* NK92MI Imaging and Biodistribution studies**

NOD.Cg-Prkdc^{SCID}Il2rg^{tm1Wjl}/SzJ (NSG) female mice were purchased from Charles River. When mice were 6 weeks old they were injected intravenously with 500,000 NK92MI cells (n=7). 2.96-4.44 MBq (10-15μg) of ^{64}Cu-NKp30Ab (n=4) or ^{64}Cu-mIgG (n=3) was injected 48 h after NK92MI cell injection. PET/CT imaging and *ex vivo* biodistribution was completed 48 h after PET tracer injection.

RESULTS

Flow cytometry and kill assays

NK cells isolated from human buffy coats were >95% CD3 negative and expressed both NKp30 and NKp46 (Fig. 1A). Primary NK cells NKp30 expression (3100 ±1400 epitopes/cell) was not significantly altered during bead activation (2140 ±1060 epitopes/cell) or via phorbol 12-myristate 13-acetate/Ionomycin (3300 ±1200 epitopes/cell) after 24 h (Fig. 1B). These results align with previous work in which ~2000 NKp30 epitopes were detected per primary human NK cell(*29*). The NK92MI cell line had 25500 ±1750 epitopes/cell while the HeLa NKp30 line had 30700 ±4200 epitopes/cell (Fig. 1B). NKp30Ab had no effect on the ability of NK92MI cells to kill the human melanoma lines MeWo and SK-Mel-28 (Supplemental Fig. 2), matching previous results with NKp30Ab(*30*).

Immunofluorescence staining of CD56, NKp30, and NKp46

With NKp30 expression validated on primary peripheral human NK cells, detecting NKp30 on tumor-infiltrating NK cells is essential for eventual translation. As flow cytometry on peripheral NK cells is defined as $CD3^{-}CD56^{+}$ was included in the IF panel. Both RCC patient samples showed co-localization of NKp30 and NKp46 on infiltrating NK cells (Fig. 2). In RCC 275, tumor cells were also positive for CD56.

Radiolabeling NKp30Ab

DOTA conjugation resulted in an average of 1.79 DOTA molecules per antibody while DFO conjugation resulted in an average of 1.59 DFO molecules per antibody (Supp. Fig. 3A-D). ^{64}Cu radiolabeling was achieved with a decay-corrected radiochemical yield of 60-75% and completed > 5 times. Purification resulted in radiochemical purity of >98%

by iTLC and HPLC and a specific activity of 0.185-0.37 MBq/μg (Supplemental Fig. 4A). ^{64}Cu-NKp30Ab was >95% stable in mouse and human serum up to 48 h at 37 ^{o}C (Supplemental Fig. 4B). ^{89}Zr radiolabeling was achieved with a decay-corrected radiochemical yield of 80-95% and completed > 5 times. Radiochemical purity of > 98% was achieved by iTLC with a specific activity of 0.074-0.185 MBq/μg (Supplemental Fig. 4C). ^{89}Zr-NKp30Ab and isotype controls were >95% stable in mouse and human serum up to 120 h at 37 ^{o}C (Supplemental Fig. 4D-E).

PET tracer *in vitro* binding assays

^{64}Cu-NKp30Ab and ^{89}Zr-NKp30Ab showed specific binding in HeLa NKp30 cells (Fig. 3A), compared to both negative cells and isotype controls. Immunoreactivities of 72.3% for ^{64}Cu-NKp30Ab and 63.8% for ^{89}Zr-NKp30Ab were achieved (Supplemental Fig. 5A-B). ^{64}Cu-NKp30Ab was further validated in both the human NK cell line NK92MI and human NK cells isolated from buffy coats and demonstrated specific *in vitro* binding ($p < 0.05$ relative to isotype control). Similarly, ^{89}Zr-NKp30Ab showed highly specific uptake in NKp30-expressing HeLa cells, compared to NKp30-negative lines and the ^{89}Zr-IgG controls (Fig. 3B-D).

***In vivo* PET and *ex vivo* biodistribution studies**

^{64}Cu-NKp30Ab PET/CT and biodistribution results demonstrated specific uptake in NKp30-expressing Hela tumor xenografts, compared to wild-type HeLa cells and isotype controls (Fig. 4A-B). *Ex vivo* biodistribution for ^{64}Cu-NKp30Ab in NKp30-expressing xenografts was 15.2 ± 4.5% ID/g, compared to 5.8 ± 1.9% ID/g for the ^{64}CuIgG control ($p < 0.05$). ^{64}Cu-NKp30Ab in the blood was 8.3 %ID/g, as expected for a full-size monoclonal antibody.

^{89}Zr-NKp30Ab PET/CT and biodistribution results also demonstrated specific uptake in NKp30-expressing xenografts, compared to wild-type HeLa cells and isotype controls (Fig. 5A-B). At 120 h, *ex vivo* biodistribution for ^{89}Zr-NKp30Ab in NKp30-expressing xenografts was 18.2 ± 4.8% ID/g, compared to 8.6 ± 2.1% ID/g for the ^{89}ZrIgG control (p <0.05). Tracer in the blood was 3.8 %ID/g, expected for a full-size antibody. At 48 h post-injection, ^{64}Cu-NKp30Ab had tumor/blood and tumor/muscle ratios of 1.92 ± 0.63 and 9.84 ± 6.1 respectively, while at 120 h post-injection, ^{89}Zr-NKp30Ab had tumor/blood and tumor/muscle ratios of 4.84 ± 0.87 and 19.72 ± 5.77 (Supplemental Fig. 6). The max-pixel ratios for ^{64}Cu-NKp30Ab/^{64}Cu-IgG, ^{89}Cu-NKp30Ab/^{89}Cu-IgG, and NKp30 positive and negative xenografts are reported in Supplementary Table 1.

To evaluate this tracer for imaging human NK cells *in vivo*, an ACT model was developed with NSG mice injected with NK92MI cells. In ACT mice at 48 h post-injection, NSG mice injected with ^{64}Cu-NKp30Ab showed increased uptake (14.9 ± 3.2% ID/g vs 7.1 ± 1.9% ID/g) in the spleen (p<0.05), and to a lesser extent the liver (10.5 ± 0.8% ID/g vs 8.0 ± 0.8% ID/g), compared to ^{64}Cu-IgG. In contrast, blood activity for ^{64}Cu-NKp30Ab was lower than ^{64}Cu-IgG (11.6 ± 0.7% ID/g vs 15.7 ± 1.5% ID/g), likely due to increased ^{64}Cu-NKp30Ab uptake in the liver and spleen. No other organs exhibited significant differences in ^{64}Cu uptake (Figs. 6A and B).

DISCUSSION

NK cells are a critical component of the immune system, especially in defense from viral and cancer threats. Molecular imaging has played a limited role to date in both pre-clinical and clinical studies of NK cells since they rely on *ex vivo* loading of imaging agents such as fluorescent dyes(*31,32*), MR contrast, SPECT tracers(*14,33*), or PET

tracers(*34,35*) into NK cells. However, these approaches are not applicable to imaging endogenous NK cells in their native environment, and also suffer from signal dilution due to cell division and death. Other methods such as PET reporter genes(*17*) have yet to be explored for NK cells and are limited to cells expanded and activated *ex vivo*.

The number of NKp30 epitopes/cell (2000-4000) indicates NKp30 expression does not significantly vary after 24 hours of activation in primary NK cells and the NK92MI cell line, making it a good general marker for NK cells. HeLa cells engineered to express NKp30 had similar levels of the NKp30 receptor as the NK92MI cell line, making it a realistic model for determining in vitro binding.

While the quantitative flow cytometry data demonstrated the receptor is expressed at levels desirable as an imaging biomarker, detecting NKp30 on tumor-infiltrating NK cells was necessary as this is one of the desired clinical applications. IF on human RCC samples showed NKp30 and NKp46 colocalization in infiltrating NK cells, demonstrating that tumor-infiltrating NK cells express the target of interest. This experiment also highlighted a major limitation of using the NK marker CD56 – tumors such as glioma and RCC can express this marker(*20*), precluding specific quantification of NK cell infiltration. With NKp30 validated as an NK cell-specific marker expressing on tumor-infiltrating NK cells, an anti-NKp30 full size antibody was radiolabeled and characterized. Both PET tracers demonstrated high specificity for NKp30-expressing HeLa cells, the human NK92MI cell line, and human NK cells isolated from buffy coats. ^{64}Cu- and ^{89}Zr- NKp30Ab demonstrated specificity and expected pharmacokinetics(*36,37*) in *in vivo* murine xenografts. While the longer half-life of ^{89}Zr ($t_{1/2}$=78.4 h) aligns better with antibodies than

^{64}Cu ($t_{1/2}$=12.7 h), both have been translated for antibody PET imaging and therefore were evaluated here.

Even with the aforementioned pharmacokinetic limitations, ^{64}Cu-NKp30Ab was able to image ACT in an NSG model, with injected NK cells (NK92MI) residing in the spleen and liver quantified at 48 h post-injection. NK cells in immunodeficient mice home to the spleen, matching previous results(*38,39*). These results demonstrate the PET probe can image the migrating of human NK cells *in vivo*, an essential prerequisite for potential translation. To further investigate this possibility, the effect of the NKp30Ab on NK cells ability to kill melanoma cells was tested *in vitro* and had no deleterious effect. This aligns with previous reports that multiple activating receptors need to be simultaneously engaged to surpass the activation threshold(*40*).

While this study develops and validates PET imaging tools for NK cells, there are limitations to address in future studies. Since NKp30 is not expressed by murine NK cells, and therefore a murine version of this probe could not be assessed in immunocompetent mice. To address this, NK cells were injected into NSG mice followed by the NKp30Ab PET probe, which demonstrated the ability to quantitatively image these cells. Xenografts of transfected HeLa cells expressing NKp30 in *nu/nu* mice were used and had a similar concentration of cell-surface NKp30 receptors as the NK92MI cell line, but a log order higher than that of primary NK cells. While the low number of NK cells that typically infiltrate tumors is a potential challenge(*41*), the IF presented here demonstrate that tumor-infiltrating NK cells do express NKp30. Future work testing this PET imaging probe in tumor-bearing, humanized immune models will elucidate levels of sensitivity and the ability to predict and monitor therapeutic response to immune-targeting therapies.

CONCLUSION

The current work quantified NK cell receptors in primary human NK cells and NK cell lines used in clinical trials and detected the presence of NKp30-expressing, tumor-infiltrating NK cells in human cancer patients. NKp30 PET tracers labeled with ^{64}Cu or ^{89}Zr both demonstrated specificity *in vivo*, with ^{89}Zr-NKp30Ab exhibiting superior *in vivo* contrast at their respective optimal timepoints. The distribution of NK cells in an ACT mouse model was quantified using ^{64}Cu-NKp30Ab. Our data support continued development of NK cell-specific PET tracers for imaging response during NK cell therapies that are currently being investigated in the clinic.

DISCLOSURE

The costs of publication of this article were defrayed in part by the payment of page charges. Therefore, and solely to indicate this fact, this article is hereby marked “advertisement” in accordance with 18 USC section 1734. No other potential conflicts of interest relevant to this article exist.

ACKNOWLEDGEMENTS

This work was supported by a Cancer-Translational Nanotechnology Training grant (T32 CA196585 to TMS), a Swiss National Science Foundation Postdoc Mobility Fellowship (P400PM_183915 to CMS), the Ben and Catherine Ivy Foundation (SSG) and the Canary Foundation (SSG), and a Stanford Bio-X seed grant (SSG). Small animal PET/CT imaging and gamma counter measurements were performed at the Stanford Center for *In Vivo* Imaging (SCi^3). We thank Sarah Black for performing immunofluorescence staining of RCC samples.

KEY POINTS

QUESTION: Is NKp30 a valid PET imaging biomarker for human NK cells?

PERTINENT FINDINGS: NKp30 had consistent expression on human NK cells from various donors and is expressed on tumor-infiltrating NK cells in human RCC. While both ^{64}Cu- and ^{89}Zr- NKp30Ab PET probes had high stability, specificity, and immunoreactivity, ^{89}Zr-NKp30Ab showing statistically significant target-to-background PET signals at optimal imaging timepoints. ^{64}Cu-NKp30Ab demonstrated the ability to image adoptive cell transfer of NK cells in NSG mice.

IMPLICATIONS FOR PATIENT CARE: Our NK cell PET diagnostic probes have the potential for measuring *in vivo* NK tumor infiltration in upcoming therapeutic NK cell trials.

REFERENCES

1. Yang Y. Cancer immunotherapy: Harnessing the immune system to battle cancer. *J Clin Invest.* 2015;125:3335-3337.

2. Wolchok JD, Chiarion-Sileni V, Gonzalez R, et al. Overall survival with combined nivolumab and ipilimumab in advanced melanoma. *N Engl J Med.* 2017;377:1345-1356.

3. Dusetzina SB. Drug pricing trends for orally administered anticancer medications reimbursed by commercial health plans, 2000-2014. *JAMA Oncol.* 2016;2:960-961.

4. Postow MA, Sidlow R, Hellmann MD. Immune-related adverse events associated with immune checkpoint blockade. *N Engl J Med.* 2018;378:158-168.

5. Shapovalova M, Pyper SR, Moriarity BS, LeBeau AM. The molecular imaging of natural killer cells. *Mol Imaging.* 2018;17:1536012118794816.

6. Rezvani K, Rouce R, Liu E, Shpall E. Engineering natural killer cells for cancer immunotherapy. *Mol Ther.* 2017;25:1769-1781.

7. Muntasell A, Ochoa MC, Cordeiro L, et al. Targeting nk-cell checkpoints for cancer immunotherapy. *Curr Opin Immunol.* 2017;45:73-81.

8. Guillerey C, Huntington ND, Smyth MJ. Targeting natural killer cells in cancer immunotherapy. *Nat Immunol.* 2016;17:1025-1036.

9. Fehniger TA, Cooper MA. Harnessing nk cell memory for cancer immunotherapy. *Trends Immunol.* 2016;37:877-888.

10. Lopez-Soto A, Gonzalez S, Smyth MJ, Galluzzi L. Control of metastasis by nk cells. *Cancer Cell.* 2017;32:135-154.

11. Ochoa MC, Minute L, Rodriguez I, et al. Antibody-dependent cell cytotoxicity: Immunotherapy strategies enhancing effector nk cells. *Immunol Cell Biol.* 2017;95:347-355.

12. Klingemann H. Challenges of cancer therapy with natural killer cells. *Cytotherapy.* 2015;17:245-249.

13. Krasnova Y, Putz EM, Smyth MJ, Souza-Fonseca-Guimaraes F. Bench to bedside: Nk cells and control of metastasis. *Clin Immunol.* 2017;177:50-59.

14. Meller B, Frohn C, Brand JM, et al. Monitoring of a new approach of immunotherapy with allogenic (111)in-labelled nk cells in patients with renal cell carcinoma. *Eur J Nucl Med Mol Imaging.* 2004;31:403-407.

15. Levy E, Reger R, Segerberg F, et al. Enhanced bone marrow homing of natural killer cells following mrna transfection with gain-of-function variant cxcr4(r334x). *Front Immunol.* 2019;10:1262.

16. Sato N, Wu H, Asiedu KO, Szajek LP, Griffiths GL, Choyke PL. (89)zr-oxine complex PET cell imaging in monitoring cell-based therapies. *Radiology.* 2015;275:490-500.

17. Keu KV, Witney TH, Yaghoubi S, et al. Reporter gene imaging of targeted t cell immunotherapy in recurrent glioma. *Sci Transl Med.* 2017;9.

18. Galli F, Rapisarda AS, Stabile H, et al. In vivo imaging of natural killer cell trafficking in tumors. *J Nucl Med.* 2015;56:1575-1580.

19. Uhlen M, Fagerberg L, Hallstrom BM, et al. Proteomics. Tissue-based map of the human proteome. *Science.* 2015;347:1260419.

20. The human protein atlas. 2020.02.07.

21. De Maria A, Bozzano F, Cantoni C, Moretta L. Revisiting human natural killer cell subset function revealed cytolytic cd56(dim)cd16+ nk cells as rapid producers of abundant ifn-gamma on activation. *Proc Natl Acad Sci U S A.* 2011;108:728-732.

22. Kruse PH, Matta J, Ugolini S, Vivier E. Natural cytotoxicity receptors and their ligands. *Immunol Cell Biol.* 2014;92:221-229.

23. Li Y, Mariuzza RA. Structural basis for recognition of cellular and viral ligands by nk cell receptors. *Front Immunol.* 2014;5:123.

24. Chretien AS, Fauriat C, Orlanducci F, et al. Nkp30 expression is a prognostic immune biomarker for stratification of patients with intermediate-risk acute myeloid leukemia. *Oncotarget.* 2017;8:49548-49563.

25. Han B, Mao FY, Zhao YL, et al. Altered nkp30, nkp46, nkg2d, and dnam-1 expression on circulating nk cells is associated with tumor progression in human gastric cancer. *J Immunol Res.* 2018;2018:6248590.

26. Garcia-Iglesias T, Del Toro-Arreola A, Albarran-Somoza B, et al. Low nkp30, nkp46 and nkg2d expression and reduced cytotoxic activity on nk cells in cervical cancer and precursor lesions. *BMC Cancer.* 2009;9:186.

27. Schürch CM, Bhate SS, Barlow GL, et al. Coordinated cellular neighborhoods orchestrate antitumoral immunity at the colorectal cancer invasive front. *bioRxiv.* 2019:743989.

28. Lindmo T, Boven E, Cuttitta F, Fedorko J, Bunn PA, Jr. Determination of the immunoreactive fraction of radiolabeled monoclonal antibodies by linear extrapolation to binding at infinite antigen excess. *J Immunol Methods.* 1984;72:77-89.

29. Dorsch M, Urlaub D, Bonnemann V, Brode P, Sandusky M, Watzl C. Quantitative analysis of human nk cell reactivity using latex beads coated with defined amounts of antibodies. *Eur J Immunol.* 2020;50:656-665.

30. Vacca P, Cantoni C, Prato C, et al. Regulatory role of nkp44, nkp46, dnam-1 and nkg2d receptors in the interaction between nk cells and trophoblast cells. Evidence for divergent functional profiles of decidual versus peripheral nk cells. *Int Immunol.* 2008;20:1395-1405.

31. Tavri S, Jha P, Meier R, et al. Optical imaging of cellular immunotherapy against prostate cancer. *Mol Imaging.* 2009;8:15-26.

32. Lim YT, Cho MY, Noh YW, Chung JW, Chung BH. Near-infrared emitting fluorescent nanocrystals-labeled natural killer cells as a platform technology for the optical imaging of immunotherapeutic cells-based cancer therapy. *Nanotechnology.* 2009;20:475102.

33. Matera L, Galetto A, Bello M, et al. In vivo migration of labeled autologous natural killer cells to liver metastases in patients with colon carcinoma. *J Transl Med.* 2006;4:49.

34. Melder RJ, Brownell AL, Shoup TM, Brownell GL, Jain RK. Imaging of activated natural killer cells in mice by positron emission tomography: Preferential uptake in tumors. *Cancer Res.* 1993;53:5867-5871.

35. Meier R, Piert M, Piontek G, et al. Tracking of [18f]fdg-labeled natural killer cells to her2/neu-positive tumors. *Nucl Med Biol.* 2008;35:579-588.

36. Deri MA, Zeglis BM, Francesconi LC, Lewis JS. PET imaging with (8)(9)zr: From radiochemistry to the clinic. *Nucl Med Biol.* 2013;40:3-14.

37. Rice SL, Roney CA, Daumar P, Lewis JS. The next generation of positron emission tomography radiopharmaceuticals in oncology. *Semin Nucl Med.* 2011;41:265-282.

38. Miller JS, Rooney CM, Curtsinger J, et al. Expansion and homing of adoptively transferred human natural killer cells in immunodeficient mice varies with product preparation and in vivo cytokine administration: Implications for clinical therapy. *Biol Blood Marrow Transplant.* 2014;20:1252-1257.

39. Cany J, van der Waart AB, Tordoir M, et al. Natural killer cells generated from cord blood hematopoietic progenitor cells efficiently target bone marrow-residing human leukemia cells in nod/scid/il2rg(null) mice. *PLoS One.* 2013;8:e64384.

40. Long EO, Kim HS, Liu D, Peterson ME, Rajagopalan S. Controlling natural killer cell responses: Integration of signals for activation and inhibition. *Annu Rev Immunol.* 2013;31:227-258.

41. Gauthier L, Morel A, Anceriz N, et al. Multifunctional natural killer cell engagers targeting nkp46 trigger protective tumor immunity. *Cell.* 2019;177:1701-1713 e1716.

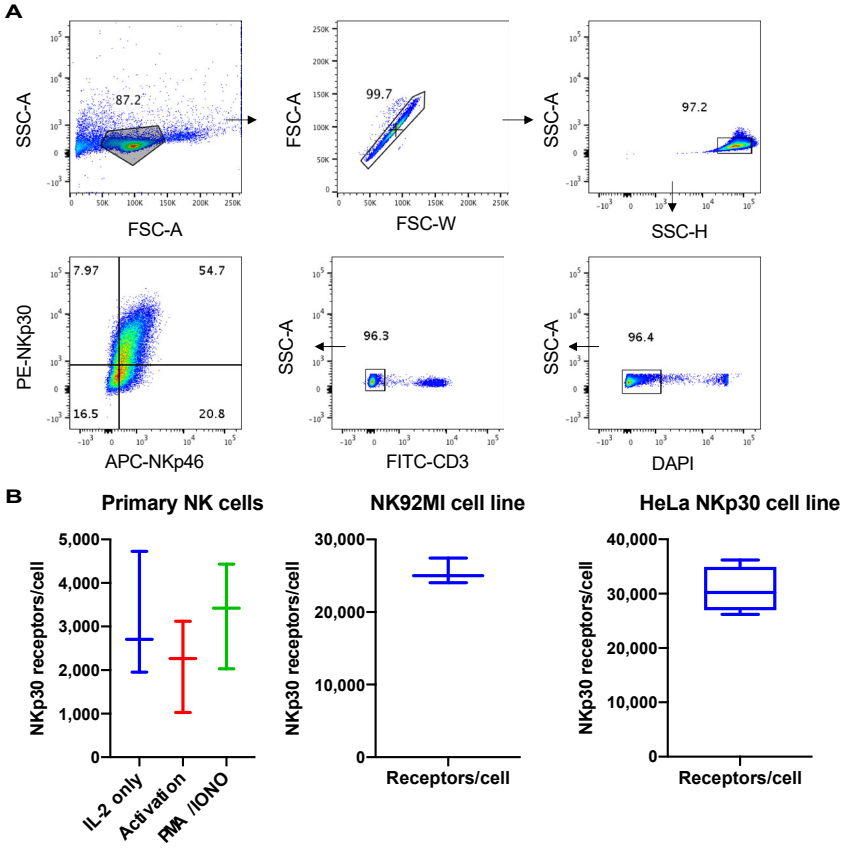

Figure 1. Flow cytometry on primary human NK cells. A) Gating strategy to delineate human NK cells isolated from human buffy coats. B) Quantification of the NKp30 receptor on primary human NK samples, the NK92MI human NK cell line, and the transfected HeLa/NKp30 line (n=3 per condition, mean and SD shown). Primary NK cells were activated for 24 h with activation beads or Phorbol 12-myristate 13-acetate/Ionomycin.

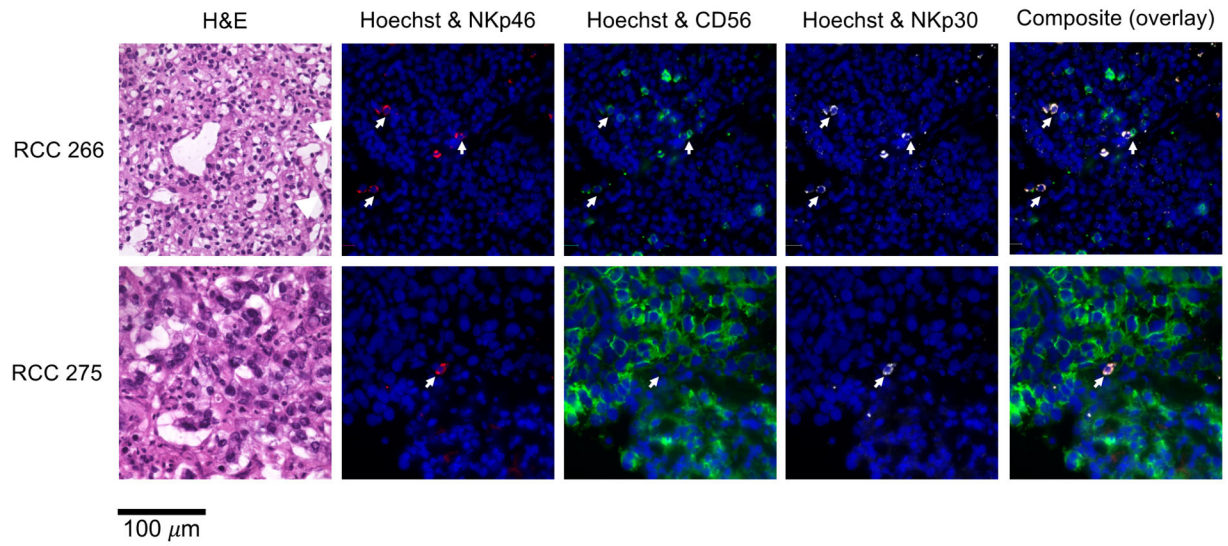

Figure 2. Detection of infiltrating human NK cells expressing NKp30 in RCC samples. RCC samples were stained with Hoechst 33342, AF488-NKp46, PE-CD56, and APC-NKp30. Both samples had infiltrating NK cells that co-stained for NKp46 and NKp30, denoted by white arrows. Tumor cells in RCC 275 were also positive for CD56, demonstrating a limitation in specificity of this common marker for detection of peripheral NK cell staining.

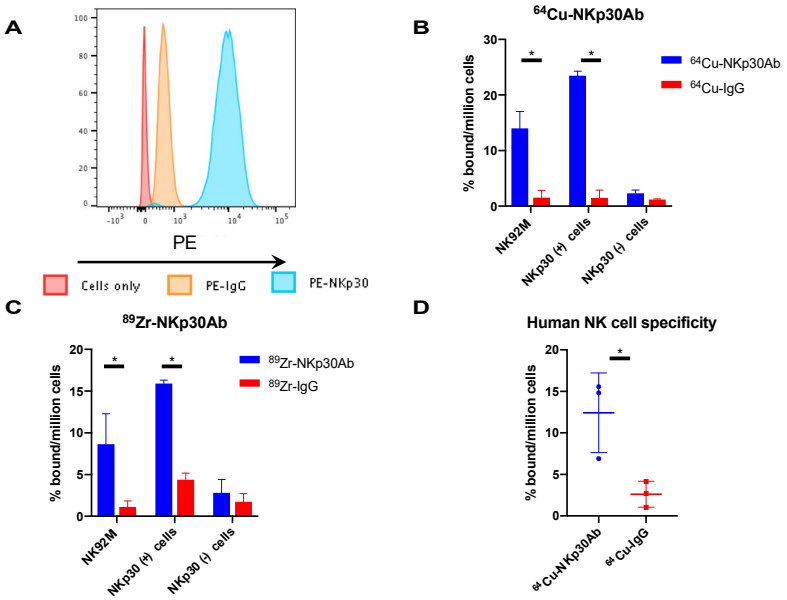

Figure 3. *In vitro* specificity for ^{64}Cu-NKp30Ab and ^{89}Zr-NKp30Ab. A) Flow cytometry of NKp30-expressing HeLa cells. B) ^{64}Cu-NKp30Ab shows high specificity for Hela cells expressing the NKp30 receptor and the NK92MI human NK cell line, in comparison with the NKp30-negative cell lines and isotype controls (n=3). C) ^{89}Zr-NKp30Ab shows high specificity for Hela cells expressing the NKp30 receptor and the NK92MI human NK cell line, in comparison with the NKp30-negative cell lines and isotype controls (n=3). D) ^{64}Cu-NKp30Ab shows specific uptake at 30 min post incubation in isolated and *ex vivo* activated human NK cells isolated from buffy coats, compared to isotype control (n=3). * denotes $p<0.05$.

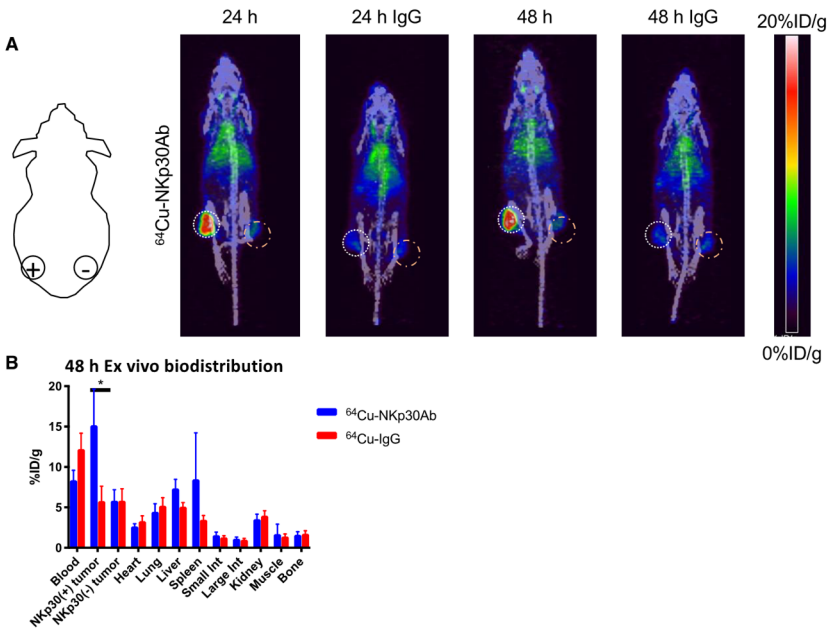

Figure 4. *In vivo* ^{64}Cu-NKp30Ab PET/CT imaging of NKp30 expression in tumor xenografts and *ex-vivo* biodistribution study. A) ^{64}Cu-NKp30Ab and ^{64}Cu-IgG PET/CT imaging completed at 24- and 48-h post-injection (n=10, 3 separate cohorts). The left flank has NKp30-expressing HeLa cell xenografts (+, white dotted circle), while the right flank has wild-type HeLa cell xenografts without NKp30 expression (-, orange dashed circle). B) Biodistribution of ^{64}Cu-NKp30Ab and ^{64}Cu-IgG at 48 h post-injection (n=10, 3 separate cohorts). * denotes $p<0.05$, mean and standard deviation shown here.

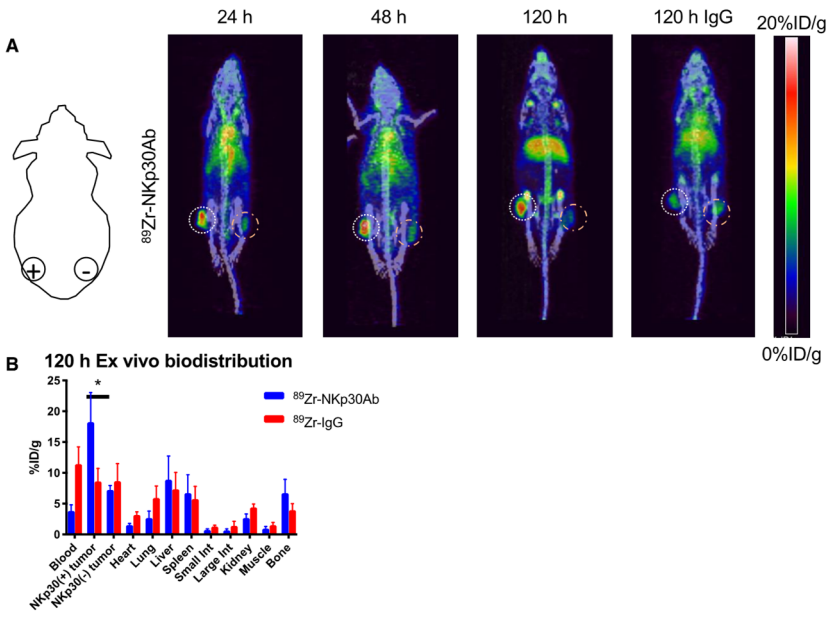

Figure 5. *In vivo* ^{89}Zr-NKp30Ab PET/CT imaging of NKp30 expression in tumor xenografts and *ex-vivo* biodistribution study. A) ^{89}Zr-NKp30Ab imaging at 24, 48, and 120 h post-injection (n=7). ^{89}Zr-IgG PET/CT imaging at 120 h post-injection is shown as a comparison (n=7). The left flank has NKp30-expressing HeLa cell xenografts (+, white dotted circle), while the right flank has wild-type HeLa cell xenografts without NKp30 expression (-, orange dashed circle). B) Biodistribution of ^{89}Zr-NKp30Ab and ^{89}Zr-IgG at 120 h post-injection (n=7, 2 separate cohorts). * denotes $p<0.05$, mean and standard deviation shown here.

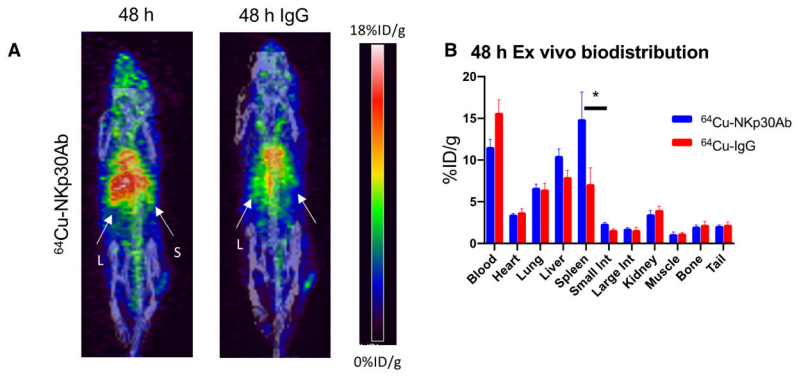

Figure 6. *In vivo* ^{64}Cu-NKp30Ab immunoPET and *ex-vivo* biodistribution study in an adoptive cell transfer model of NK cells injected intravenously in NSG mice. A) ^{64}Cu-NKp30Ab and ^{64}Cu-IgG PET/CT imaging completed at 48 h post-injection (n=3-4). Higher liver and spleen uptake are seen for ^{64}Cu-NKp30Ab compared to ^{64}Cu-IgG due to the presence of NK92MI cells. L denotes liver, S denotes spleen. B) Biodistribution of ^{64}Cu-NKp30Ab and ^{64}Cu-IgG at 48 h post-injection (n=3-4). * denotes $p<0.05$, mean and standard deviation are shown.

Supporting Information

PET imaging of the natural killer cell activation receptor NKp30

Travis M. Shaffer[1], Amin Aalipour[2], Christian M. Schürch[3], Sanjiv S. Gambhir[1,2,4,*]

1. Department of Radiology, Stanford University, Stanford CA, 94305
2. Department of Bioengineering, Stanford University, Stanford CA, 94305
3. Department of Microbiology & Immunology, Stanford University, Stanford, CA, 94305
4. Bio-X Program and Molecular Imaging Program at Stanford (MIPS), Stanford University, Stanford CA, 94305

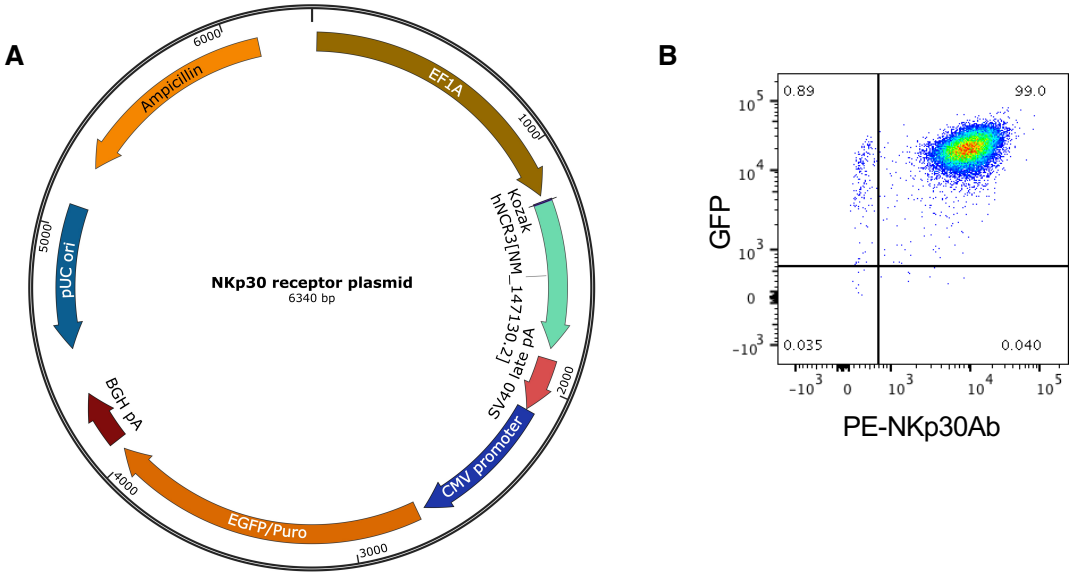

Supplemental Figure 1. Engineering of NKp30-expressing HeLa cells. **A)** The plasmid used for NKp30 transfection and puromycin (Puro)selection of stable cells. **B)** Flow cytometry analysis on stably transfected HeLa cells after 3 rounds of cell sorting (top 2% GFP and NKp30 positive cells for each round).

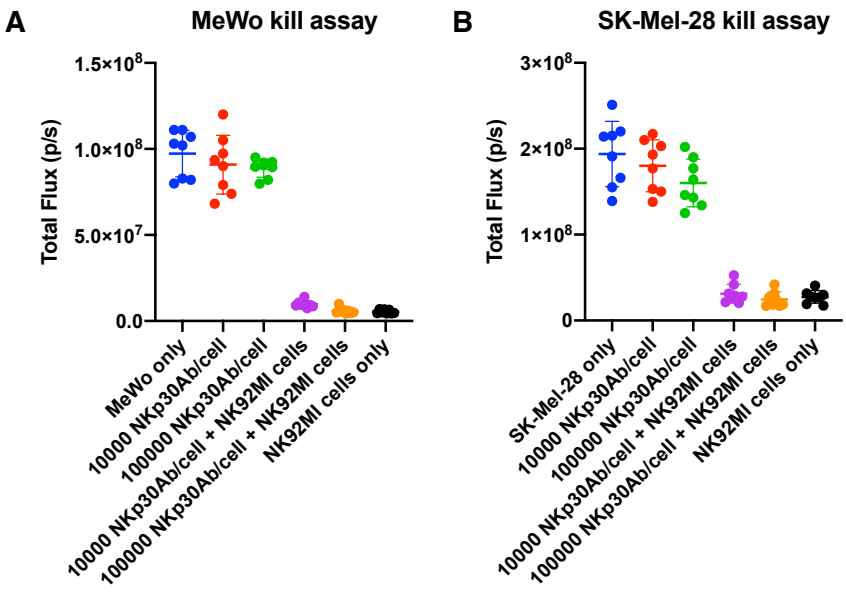

Supplemental Figure 2. NK92MI kill assay. **A)** NKp30Ab had no effect on the killing efficacy of human NK cell line NK92M for MeWo cells (expressing fluc). NKp30Ab was added at two different concentrations to NK92M cells, along with MeWo cells at 1:1 ratio. The FL signals in MeWo cells were imaged at 24 h, n=8 wells/condition. **B)** NK cell kill assay with SK-Mel-28 cells (expressing fluc) as described in (A).

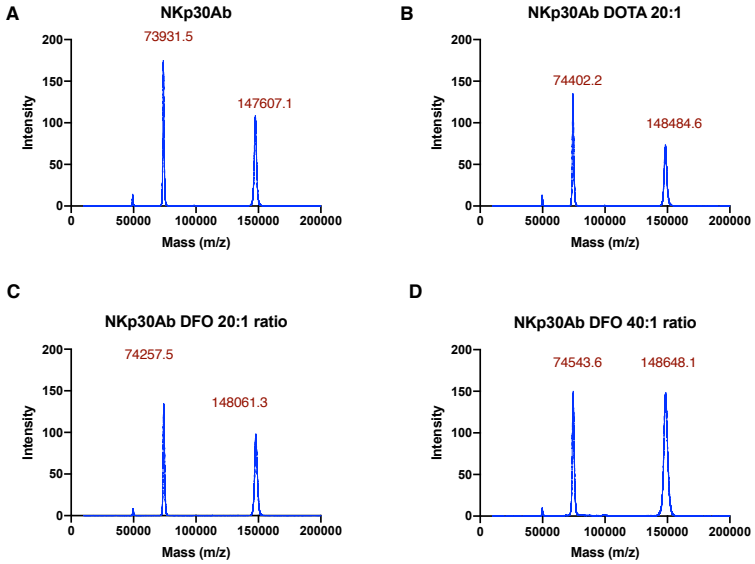

Supplemental figure 3. Representative MALDI-MS results for unconjugated NKp30Ab (A), DOTA-NKp30Ab (B) and DFO-NKp30Ab (C & D).

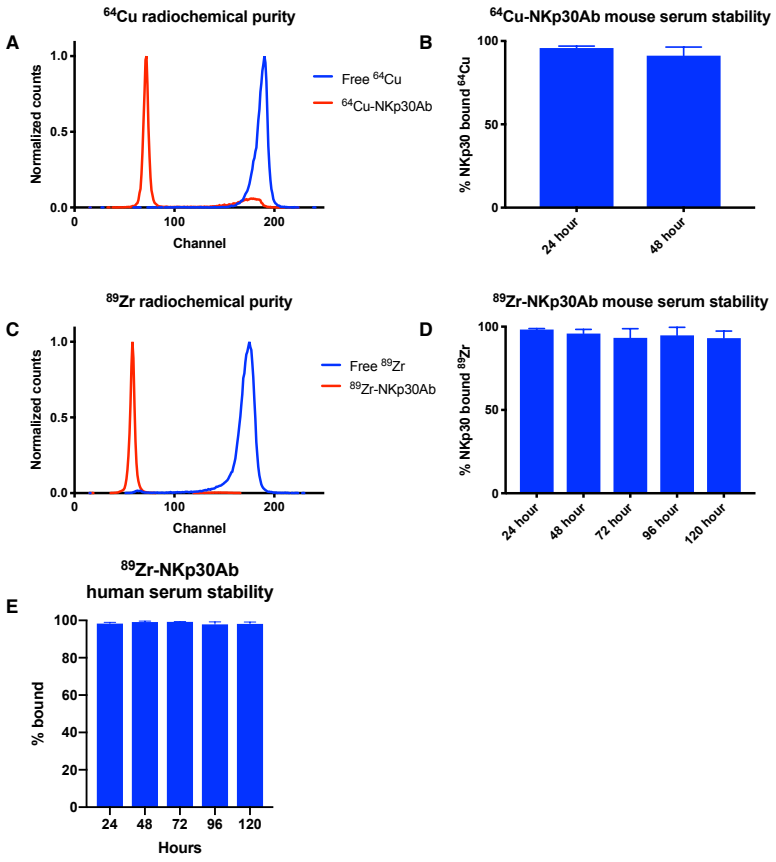

Supplemental figure 4. Radiochemical evaluation for ^{64}Cu-NKp30Ab and ^{89}Zr-NKp30Ab. **A)** Representative iTLC of free ^{64}Cu and purified ^{64}Cu-NKp30Ab. **B)** Mouse serum stability of ^{64}Cu-NKp30Ab at 37 ^{o}C at 24 and 48 h, n=5. **C)** Representative iTLC of free ^{89}Zr and purified ^{89}Zr-NKp30Ab. **D)** Mouse serum stability of ^{89}Zr-NKp30Ab at 37 ^{o}C at different time points (24 to 120 h), n=5. **E)** ^{89}Zr-NKp30Ab was stable in human serum at 37 ^{o}C for at least 120 hours (n=3).

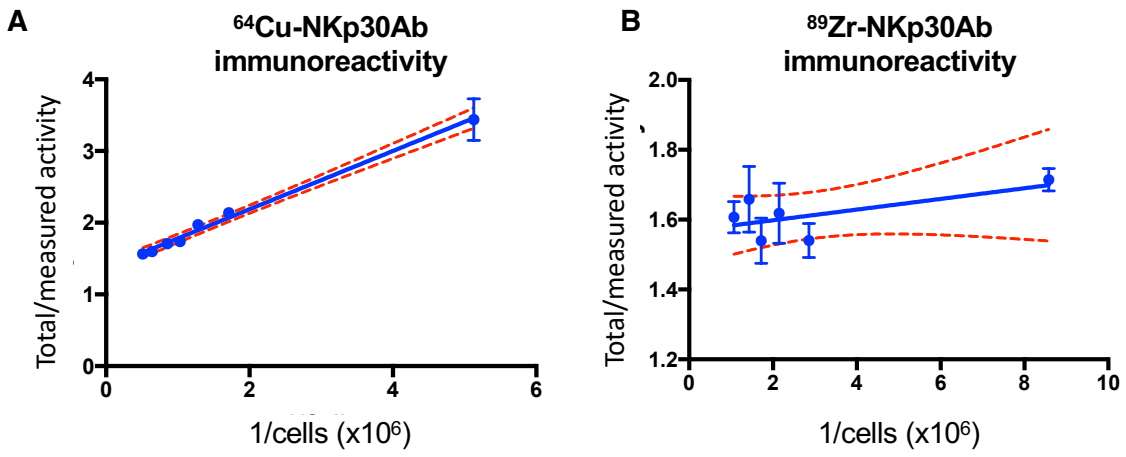

Supplemental figure 5. *In vitro* characterization of immunoPET probes. **A)** ^{64}Cu-NKp30Ab immunoreactivity was determined to be 72.7% via a Lindmo Assay (n=3). **B)** ^{89}Zr-NKp30Ab immunoreactivity was determined to be 63.8% via a Lindmo Assay (n=3).

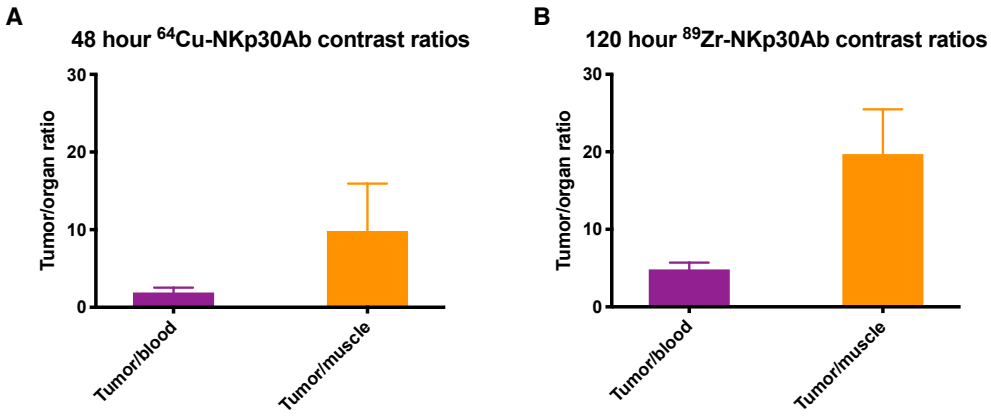

Supplemental Figure 6. Evaluation of ^{64}Cu-NKp30Ab uptake compared to that of ^{89}Zr-NKp30Ab at the optimal time point for each tracer in Hela cells xenografts stably expressing NKp30. **A)** Tumor to organ contrast ratios for ^{64}Cu-NKp30Ab at 48 h (n= 10). **B)** Tumor to organ contrast ratios for ^{89}Zr-NKp30Ab at 120 h (n= 7).

Supplemental Table 1. PET ROI Pixel ratios, Figure 5 and 6	
ROI quantification ratios	**Maximum pixel ratio**
^{64}Cu-NKp30Ab/^{64}Cu-IgG 48 h	3.13 +/- 0.75
^{64}Cu-NKp30Ab injection NKp30^{+} tumor/NKp30^{-} tumor 48 h	3.09 +/- 0.54
^{89}Zr-NKp30Ab/^{89}Zr-IgG 120 h	2.19 +/- 0.38
^{89}Zr-NKp30Ab injection NKp30^{+} tumor/NKp30^{-} tumor 120 h	2.82 +/- 0.65